

# A Perspective on the State of Aerospace Computational Fluid Dynamics Technology

Mori Mani<sup>1</sup> and Andrew J. Dorgan<sup>2</sup>

<sup>1</sup>Aerospace Computational Design Laboratory, Massachusetts Institute of Technology, Cambridge, Massachusetts, USA; email: mmani@mit.edu

<sup>2</sup>The Boeing Company, St. Louis, Missouri, USA

## ANNUAL REVIEWS CONNECT

[www.annualreviews.org](http://www.annualreviews.org)

- Download figures
- Navigate cited references
- Keyword search
- Explore related articles
- Share via email or social media

Annu. Rev. Fluid Mech. 2023. 55:431–57

The *Annual Review of Fluid Mechanics* is online at [fluid.annualreviews.org](http://fluid.annualreviews.org)

<https://doi.org/10.1146/annurev-fluid-120720-124800>

Copyright © 2023 by the author(s). This work is licensed under a Creative Commons Attribution 4.0 International License, which permits unrestricted use, distribution, and reproduction in any medium, provided the original author and source are credited. See credit lines of images or other third-party material in this article for license information.



## Keywords

computational fluid dynamics, aerospace CFD, industrial CFD challenges, CFD future

## Abstract

Over the past several decades, computational fluid dynamics has been increasingly used in the aerospace industry for the design and study of new and derivative aircraft. In this review we survey the CFD application process and note its place and importance within the everyday work of industry. Furthermore, the centrality of geometry and importance of turbulence models, higher-order numerical algorithms, output-based mesh adaptation, and numerical design optimization are discussed. Challenges in each area are noted and specific suggestions for investment are made. The review concludes with an outlook toward a future in which certification by analysis and model-based design are standard practice, along with a reminder of the steps necessary to lead the industry there.

## 1. INTRODUCTION

### RANS:

Reynolds-averaged  
Navier–Stokes

The aerospace industry continually searches for new technologies to provide better products at reduced costs and time to market. Computational fluid dynamics (CFD) is one such pivotal technology that the aerospace industry has invested in, shepherding its development and maturation, and the industry has now witnessed the returns in terms of invaluable, and routine, application. Prior to the 1960s, analytical methods combined with wind tunnel and flight test data were used to guide aircraft design. Analytical methods were well developed, including the Kutta–Joukowski theorem and Prandtl's lifting-line theory. The slender wing theory and linearized supersonic theory of Jones (1946) and Hayes (1947), respectively, were used in aerospace applications. These methods, while incredibly valuable, result from substantial simplifications of the governing equations of fluid dynamics and therefore necessitated augmentation by empirical data to arrive at adequate system performance predictions.

The advent of computing technology with sufficient power to solve less simplified forms of the governing equations of fluid dynamics gave rise to numerical methods and modern CFD in the early 1960s. As a result, panel methods were developed for predicting the lift of bodies using the linearized potential equations (Jameson 1987, Johnson et al. 2005). These included both 2D and 3D formulations, which were used to improve wing design and aircraft mission performance (Rubbert 1994) as a whole.

In the 1970s numerical algorithms for inviscid and viscous flows were being developed, and this work continued throughout the 1980s. The first major breakthrough for a simulation of transonic flow with shocks was achieved by Murman & Cole (1971) using small-disturbance theory. Later, Jameson & Caughey (1977) introduced a conservative finite-volume algorithm, which led to the development of the FLO-27/28 code for transonic flow predictions. Boeing Commercial Airplanes invested substantially in the maturation of this code, coupling it with the mesh generation capability of Thompson et al. (1974) and a boundary layer code, A411 (McLean & Randall 1979), for wing–body–nacelle design. This capability was a major workhorse at Boeing until the early 1990s. During this same period, a full potential flow solver coupled with a boundary layer solver, P582, was developed at Boeing for propulsion analyses (Reyhner 1981).

In the early 1980s, the X3D (Cosner 1985) RANS (Reynolds-averaged Navier–Stokes) solver based on velocity-splitting was developed at McDonnell-Douglas Corporation (MDC) for fore-body and inlet analysis of military configurations. (In industry there is a sloppiness in referring to RANS capabilities as “Navier–Stokes codes” when, in most cases, a turbulence model is used to directly solve for the mean field. We perpetuate the interchangeable use of terminology in this review.) A zonal 3D mesh generation capability based on the work of Thompson et al. (1974) and Sorenson (1980) was added to the process for enhanced capability. The solver’s discretization was based on the finite-difference method. For turbulence closure it used the model of Cebeci & Smith (1974). X3D was efficient and could turn around solutions on a reasonable grid of the time (80,000 nodes) in a day on a VAX-11/780 computer. This code was used in the design and analysis of the MDC F/A-18A Hornet and AV-8B Harrier inlets, among other applications. These two aircraft became primary vehicles in the US Navy and Marine Corps, and X3D played a crucial role in their development.

Other 2D, quasi-3D, and 3D Euler and Navier–Stokes (N-S) solvers aside from X3D were also developed in the 1980s (e.g., Verhoff & O’Neil 1981), as were codes based on the full potential equation, such as Boeing’s TRANSAIR code (Johnson et al. 2005), which is an adaptive unstructured mesh solver with coupling to an integral boundary layer method. TRANSAIR is a valuable tool with significant capabilities to handle complex geometries for lift and drag prediction at cruise conditions, as well as in conditions with small regions of flow separation. It continues to be used today, primarily in commercial wing design and assessment, owing to its accuracy and efficiency.

Despite its value, TRANAIR is not a general-purpose flow solver and, thus, other methods have also been developed and employed within Boeing (Buning et al. 1988, Kamenetskiy et al. 2014) that are better suited to analyzing a larger portion of the flight envelope and for treating supersonic flows.

Many of the Euler and N-S solvers leveraged the developments of the finite-volume method. Jameson et al.'s (1981) finite-volume algorithms, van Leer's (1979) MUSCL (monotonic upstream-centered scheme for conservation laws), and Roe's (1981) approximate Riemann solver became the basis for many Euler and N-S solvers within government labs and the aerospace industry. Robust and accurate total variation diminishing schemes were devised that allowed for convergence in the presence of discontinuities without reverting to global first-order accuracy (Chakravarthy et al. 1985). While finite-difference methods lend themselves well to structured mesh algorithms and higher-order methods, the finite-volume method more naturally incorporates the principles of conservation of mass, momentum, and energy (consistent with physics) and handles discontinuities by using the integral form of the governing equations. Over time, codes using these techniques became dominant for industrial CFD applications.

With the computing power brought by Cray Research (X-MP and Y-MP supercomputers) from the mid-1980s to the early 1990s, it was possible to simulate wing–body–nacelle configurations and predict unsteady flow behavior for aircraft components. Some of the notable solvers developed during this period were CFL3D (Computational Fluids Laboratory 3D) by NASA Langley Research Center (NASA-LaRC) (Vatsa et al. 1989), NASTD (Navier–Stokes Three Dimensional) by MDC (Bush 1988), USA (Unified Solution Algorithms) by Rockwell (Chakravarthy et al. 1985), and OVERFLOW by NASA Ames Research Center (Buning et al. 1988). These solvers generally utilized structured grid topologies, organized in multiple blocks/domains, that either abutted or overlapped each other. These N-S solvers were adopted by the aerospace industry but could not be used as a design tool due to still insufficient computational power; they were instead primarily used for risk mitigation and addressing issues observed in wind tunnel data. The codes were primarily used by CFD experts, as opposed to program/project engineers, and regularly suffered from robustness issues. Their use was limited by the lack of robust closure (i.e., turbulence) models, their lack of residual convergence, their tedious requirements on grid quality, and their long solution times; however, they shed light on the possibilities awaiting the field and spurred continued investment.

In the 1990s and 2000s, the aerospace industry regularly applied 3D RANS codes under conditions seen by an aircraft in cruise. CFD was also used heavily in design optimization, risk mitigation, augmentation of wind tunnel data (e.g., including the impact of model distortion or wind tunnel wall interference, providing Reynolds number corrections from model to flight scale), and diagnosing observations from flight tests [e.g., F/A-18E/F asymmetrical lift loss, also known as wing drop (Stookey 2001)]. CFD technology made significant contributions in aircraft design and became a synergistic tool with wind tunnel and flight tests.

To further accelerate advancement of the CFD capability at affordable cost, in 1997 NASA Glenn Research Center (NASA-GRC), Arnold Engineering Development Complex (AEDC), and Boeing Defense, Space & Security (BDS) (then McDonnell-Douglas) merged their CFD capabilities into a single CFD solver named Wind. The Wind code was the merger of the technologies from NPARC (NASA Program for Applications-Oriented Research in CFD) (an AEDC and NASA-GRC alliance) (Power et al. 1995), NXAIR (AEDC) (Tramel et al. 1997), and NASTD (BDS) (Bush 1988), and it was based on the framework of NASTD. This merger, under the NPARC Alliance, led to a powerful CFD-solver with significantly increased capabilities over its predecessors. It was based on the finite-volume method; included complex boundary conditions for modeling screens and actuator disks; solved the Euler, parabolized N-S, thin-layer N-S, or N-S

equations; used grid sequencing for convergence acceleration; and supported a variety of gas models ranging from calorically perfect through multispecies chemistry (Bush et al. 1998). Wind featured a parallelization model that was applicable to heterogeneous computing architectures (i.e., not all hardware used in a simulation had to be identical) and included fault tolerance. The CFF (common file format) similar to, but developed earlier than the CGNS (CFD general notation system) file format, was used throughout the entire CFD process (from grid generation to postprocessing) for machine portability. The Wind code enabled collaborative CFD development among government and industry partners. As a result, detailed documentation of the code for developers and application users was created, best practices were devised, verification and validation (V&V) test cases were gathered, and the capabilities of the code were rapidly expanded. Wind highlighted the importance of CFD in aircraft design to the Department of Defense customers and served as a case study in the creation of the CREATE-AV CFD software for defense product evaluations.

While Wind was an accurate and successful CFD tool, structured gridding around complex shapes is quite time-consuming. In an effort to minimize grid generation time and accelerate the overall CFD process, Boeing developed and matured unstructured mesh technology during the early 2000s. Mesh mechanics and flow solvers were built, including the finite-volume code BCFD (Boeing CFD) (Mani et al. 2004, Cary et al. 2009) and the finite-element code GGNS (generalized geometry Navier–Stokes) (Kamenetskiy et al. 2014). Portions of BCFD were used to extend Wind to accommodate unstructured meshes, resulting in the birth of Wind-US. Other elements, including the mesh mechanics/grid generation capability and boundary layer transition modeling, were retained as proprietary to Boeing. BCFD has continued to evolve and improve through active development to enable adjoint-based shape optimization, to support and utilize mesh adaptation, to exercise numerous scale-resolving methods, and to adapt to advances in computing architectures. Similarly, GGNS is a robust second-order accurate finite-element RANS solver focused on ensuring numerical iterative convergence. It shares the core mesh adaptation capability, EPIC (Michal & Krakos 2012), with BCFD.

The maturation of unstructured mesh technology has fostered automation and significantly reduced the time an engineer spends on mesh generation, thus allowing a single individual to do the work that would have required a whole team of people in the past. Of course, without commensurate improvements in high-performance computing (HPC) this would be largely for naught. These advances have also expanded the use of CFD to a wider audience (a potential double-edged sword) since the expertise needed for grid generation has been lessened to a certain degree. The increased speed of grid generation, the automation of certain processes, the development of adjoint-based mesh adaptation and shape optimization, and the expanded access to significant HPC resources have brought CFD into a new era in which it is a critical and essential element of digital design and model-based engineering (MBE).

In the remainder of this review, we expand on the role and value of CFD (Section 2), discuss the modern CFD application process (Section 3), and elaborate on the evolution of current and next-generation solvers (Section 4). Section 5 discusses challenges and provides a future outlook.

## 2. THE IMPORTANCE OF CFD TO THE AEROSPACE INDUSTRY

CFD plays a critical role in the design and analysis of aerospace vehicles. Used early in the design process, CFD can reduce rework needed to insure the vehicle meets its objectives and safety-related standards. The first aircraft of Boeing Commercial Airplanes that benefited from CFD from its inception was the Boeing 777. Being the first, there were no legacy constraints on 777 that would be expected when working on a derivative design. The design leveraged multipoint inverse optimization to define detailed surface pressures and arrive at a desirable configuration

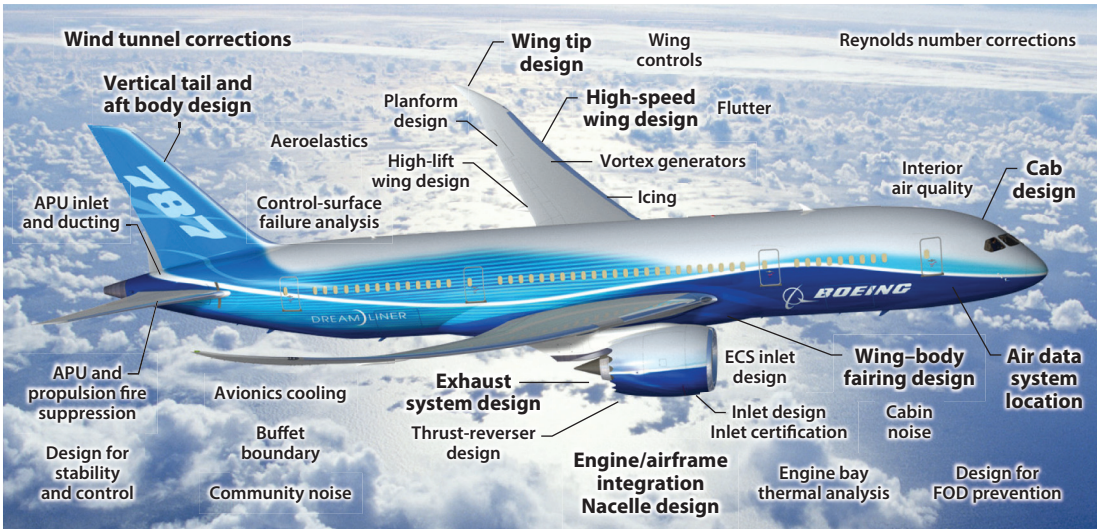


**Figure 1**

Computational fluid dynamics contributions to Boeing 787. Figure adapted from Tinoco (2008) with permission; copyright 2008 the Boeing Company. Abbreviations: APU, auxiliary power unit; ECS, environmental control system; FOD, foreign object debris.

(Tinoco 2008). Besides wing design, 777 also benefited from CFD technology in the design of the wing–body fairing, aft-body shaping, and environmental control system inlet and exhaust ports. By the time Boeing 787 was being designed, CFD capabilities had matured enough to be applied to a much broader area of the aircraft design, as highlighted in **Figure 1**.

As CFD technology has matured, it has become a standard tool of the aerospace industry alongside the wind tunnel. CFD has not, and likely will not, replace wind tunnel testing in the foreseeable future, although we have witnessed parity of these complementary methods, which both aim at a common objective: to accurately model the flight aerodynamics of an aerospace vehicle. While CFD can go from geometry to predictions of forces and moments in a matter of hours, it can take months to design and fabricate a wind tunnel model and plan the test; however, once the model is installed in the tunnel and the air is turned on, results can be rapidly collected for database generation. Unlike CFD, the wind tunnel does not suffer from potential inadequacies of grid resolution and physical modeling, among others. However, the wind tunnel does have limitations in its ability to directly predict flight. For example, it is typically unable to provide data at full flight Reynolds number, the geometry may be distorted in order to attach a support/mounting system, interference from the support system can corrupt the airflow over the geometry, and the presence of the test section walls results in a different flow field than that seen in the unbounded domain of flight. Today, corrections for these effects are often generated, in part or entirely, using CFD, further illustrating the complementary roles these techniques have assumed.

The aircraft design methodologies adopted over the last decade exhibit a specific advantage of computational methods over wind tunnel testing. Shape optimization technology and modern HPC resources have made it possible to digitally design an aircraft (not just components), leading to program-level schedule compression and cost savings, as well as a greatly reduced wind tunnel test campaign. For example, it is no longer necessary to go to the wind tunnel with a plethora of geometries to select an acceptable design. Instead, a program goes to the wind tunnel with the intent of validating an entire configuration that was first designed digitally and then optimized and initially characterized by CFD. These techniques, in part, enable the aerospace industry to tackle

challenges like the Digital Century Series (Mayfield 2020) proposed by Dr. Will Roper during his time as Assistant Secretary of the Air Force for Acquisition, Technology, and Logistics.

The value of CFD claimed above is dependent upon considerable background effort. For example, the situations described above lead to high-pressure working environments in which the engineering team cannot be burdened with concerns about the maturity of tools and processes. The tools must have been verified and validated ahead of time for the application environment in which they will be used. Additionally, processes should be well defined and robust enough that results produced by different analysts do not differ significantly. Process automation helps to address these concerns, and ideally the process should be sufficiently modular so as to allow parts to be swapped out for alternate or updated tools. Finally, documentation of the validity and range of applicability is essential to mitigate the potential for misuse. Industry must protect these tenets to confidently replicate the demonstrated contemporary successes.

### 3. THE MODERN CFD APPLICATION PROCESS

In this section we provide an overview of the industrial CFD process (see **Figure 2**). The process begins with geometry acquisition from a computer-aided design (CAD) system such as CATIA<sup>TM</sup>, Unigraphics/NX<sup>TM</sup>, or another similar product. The geometry may come in a few pieces or may comprise hundreds of thousands of elements, depending on the complexity of the configuration. Many grid generation processes require, or at least prefer, a watertight geometry in which the abutments of the various geometry components are within some small tolerance. If the CAD model is of low quality, it can require a substantial amount of effort to sew the components together while not significantly modifying the external mold line of the aircraft. While there are tools to aid in this process, such as CADfix<sup>TM</sup>, nevertheless, the quality of the geometry that comes from CAD matters. In a mature program, CAD geometry may be very detailed and intended for the manufacturing process. These geometries contain many features that are inconsequential to the fluid dynamics and ultimately need to be removed prior to grid generation to avoid unnecessary complications. This cleanup step can take many hours depending on the state of the CAD files, but we have found that this process can be accelerated by educating the CAD engineers on the requirements of the CFD process that will be employed. There is value in having a tight coupling between CAD and the mesh-generation tool in terms of process acceleration, adaptive meshing strategies, and shape optimization efforts.

Once an acceptable geometry is available, the effort turns to surface grid generation. This is the process of creating a mesh over the geometry, the vertices of which exist on the geometry surface. The densities of those mesh points in various regions of the geometry have typically been placed based on the analyst's skill/experience and heuristics; however, it is increasingly possible to hand off this responsibility to mesh-adaptation algorithms. In any event, for both structured and unstructured meshing techniques (see **Figure 3** for a graphical distinction), the standard processes used in industry rely on a so-called linear mesh (i.e., one in which the connections between the

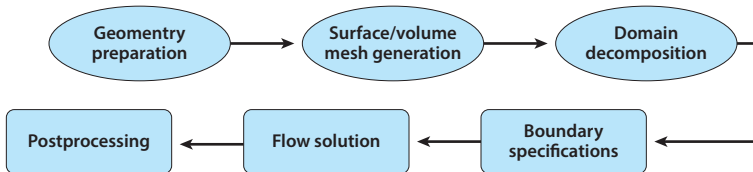


**Figure 2**

The fixed-mesh flow solution process.

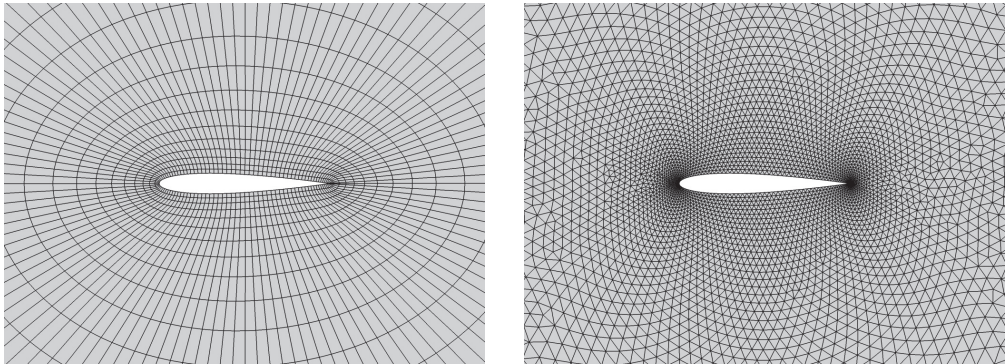


**Figure 3**

Coarse structured (*left*) and unstructured (*right*) meshes around an airfoil.

vertices are lines). Adequate representation of the geometry by the faces of the linear mesh (the areas bounded by the lines connecting the vertices) can require excessive resolution in region of high geometry curvature. Quadratic, or higher-order, meshes have an advantage in this regard, although one must not lose sight of the fact that the mesh must adequately capture the flow features around the geometry as well. Generally, taking advantage of higher-order meshes also requires a higher-order flow solution. **Figure 4** provides an example of an unstructured grid, where second- and fourth-order grids, adapted to similar levels of accuracy, are shown.

Structured meshes continue to be utilized in the industry due to highly validated and efficient N-S solvers like OVERFLOW. Structured surface mesh generation for a full aircraft configuration could take up to two weeks. On the other hand, unstructured surface mesh generation is significantly faster, taking a few hours. The decision about which approach one takes should be informed by downstream uses but is often made based on the CFD analyst's toolset familiarity/knowledge. Structured grid solvers remain in use by industry as a consequence of both of these observations.

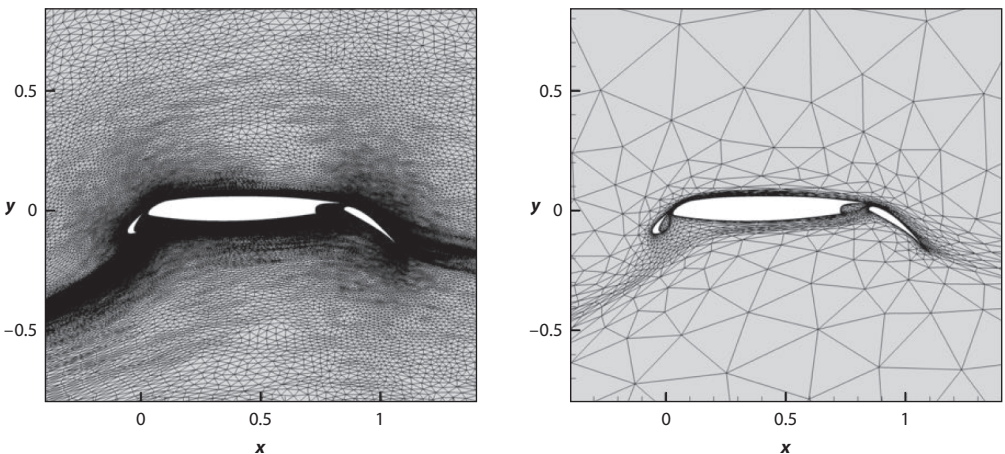


**Figure 4**

Adapted grids based on second-order (*left*) and fourth-order (*right*) solutions for a three-element airfoil; grids are adapted to a lift coefficient error of less than  $10^{-4}$ . Figure adapted from Ursachi et al. (2020) with permission; copyright 2020 the authors.

The next step in the generation of the mesh is building the volume grid, which fills the domain between the surface and far field with cells. This is a relatively simplistic process for unstructured meshes (from the view of the analyst) and can take a few minutes to several hours, depending on the complexity and size of the mesh. The algorithms for generating structured volume meshes are even faster, but, depending on the toolset, significant user intervention may be required to obtain a volume mesh of acceptable quality. A volume mesh on a complete configuration (usually exploiting lateral symmetry) may range from tens to hundreds of millions of cells (control volumes), depending on the purpose of the analysis, the quantity of interest, and the state of the flow. Flow fields with significant flow separation (e.g., flight with high angle of attack) generally require larger mesh sizes.

Following volume grid generation is the last step in mesh preparation, the specification of the boundary conditions. Boundary conditions are of course required for every boundary of the volume mesh, where the CFD simulation stops solving for the state of the flow either because the mesh has reached a physical boundary (i.e., the geometry) or because an artificial one has been imposed to terminate the extent of the computational domain. The boundary conditions involved depend on the complexity of the analysis. For example, a powered high-lift aircraft including flowing inlets and nozzles would have substantially more complex boundary specifications than a wing and fuselage configuration analysis comprising only solid walls. Common boundary conditions include those representing solid walls, symmetry planes, and far-field conditions. More complex boundary conditions can impose mass flow through an inlet or simulate the effect of porous bleed regions on the flow or even discontinuities meant to introduce the macroscopic effects of compressors, turbines, propellers, and helicopter rotors. Many variants of these are generally needed and have been amassed in industrial codes over the years.

Modern industrial CFD simulations are conducted using many compute cores (hundreds to thousands) and their associated memory. The mesh must be prepared for this distributed computing architecture, with different regions of the mesh handed off to different processors. This is generally referred to as “domain decomposition,” and there are two basic strategies taken in the toolsets. Some codes automatically handle the domain decomposition: The input to the solver is the mesh in one piece and the solution is returned at the end of the run in a similar format. Other codes (Boeing’s BCFD is one such example) can also accept a mesh that has been processed in an *a priori* domain decomposition step. Both approaches have advantages and disadvantages. While the automatic approach is convenient because it eliminates a step in the process, the alternate approach has an advantage in that postprocessing exercises can be parallelized with ease.

The grid comprises one input to the CFD solver, but many other settings are also required. Depending on the code being used, these could be made in a graphical user interface or a text-based input file. The latter takes several forms in industry, including Fortran namelists, fixed-format text files that require careful editing, and more readable keyword-driven free-format text files. There is a general desire to default as many of the inputs as possible, but sometimes a user may need to override these defaults. Other inputs, such as the flight condition, are required for every run. There is variety in how industrial aerospace CFD codes specify this basic input. A given problem can be defined by the Mach and Reynolds number of the flow, and many codes take inputs in this fashion. However, other codes also accept this specification in terms of Mach number and altitude or in terms of Mach number, pressure, and temperature. While academically redundant, these alternate specifications make it much simpler to set the properties of additional streams (e.g., the propulsion system), reducing the engineer’s workload and limiting potential error. Requiring code developers to accept inputs in a form familiar and convenient to the user pays dividends and is a highly recommended approach for any new CFD tools that may be developed for industrial applications.

The time required to obtain a RANS solution on a full aircraft configuration is of course dependent on the code used and available HPC resources; however, a solution at low angles of attack can typically be obtained within eight hours. Higher angles of attack can take longer to converge. There is potential for reducing this time by an order of magnitude by using GPUs (graphics processing units), as demonstrated by the NASA-LaRC team's FUN3D code (Walden et al. 2017) and Cascade Technologies's charLES code (Cascade Technol. 2021, Goc et al. 2021). Determining convergence of an industrial CFD application problem, with the complexities of real geometry and flow conditions, is subjective when using a finite-volume code since residual convergence to machine zero is rarely possible. Typically, convergence is declared by monitoring the evolution of the outputs of interest (e.g., forces and moments), with an eye on the residual convergence to ensure the usual behavior has been obtained. The strong linear solver techniques that are practical with the finite-element method codes (e.g., GGNS) aim to eliminate this subjectivity by striving for residual convergence on every problem. This is advantageous, but the finite-volume method will persist in industry for a long time to come due to its relative flexibility.

The final step in industrial CFD engineering analysis is postprocessing of the solutions to extract the quantities of interest and, depending on the purpose of the analysis, archive the results within the MBE system. Postprocessing may be performed using commercial tools such as FieldView<sup>TM</sup> and Tecplot<sup>TM</sup>, which are particularly powerful for solution visualization, or with specialized company-internal utilities for extracting specific sets of engineering data. For a handful of solutions in a diagnostic engineering process, this step can be performed manually for each case. However, when hundreds or thousands of solutions are to be queried, automation is a necessity for the sake of efficiency and to minimize the potential for human error. This applies not just to the final postprocessing but also to checking for convergence to an adequate level. The above automations are partially in place today for certain classes of problems. Advancing and generalizing these methods, including further integration within a program's MBE framework, will be critical as HPC hardware continues to advance, allowing for an even greater number of CFD solutions to be generated by a single user in a fixed time.

Hopefully it is obvious from the overview above that there are many opportunities (given the number of steps and choices to make) for error in this process. A well-documented and controlled process can help, but it must be flexible enough to give an engineer latitude for judgment if it is to be generally applied—this is a daunting task. In some situations, however, there is a need for ultimate rigor and control of the process since the largest risk CFD poses to aircraft design, analysis, and certification comes from the use of unverified and unvalidated tools and methods. Continued enforcement of rigor in this regard (discussed further below) must not be overshadowed by the ease with which a novice can pick up a CFD tool and produce a quality result.

## 4. EVOLUTION OF NAVIER-STOKES SOLVERS AND NEXT-GENERATION CFD TECHNOLOGIES

### 4.1. Verification and Validation

To use any design tool with confidence one needs assurance of its validity. This of course applies to CFD tools, which notoriously have many user-controlled “knobs” that can tremendously affect the resulting solution; thus, the quality of the predictions can be highly dependent on choices by the analyst. This is not meant to suggest that a given technology needs to be perfect; rather, the accuracy bounds need to be understood and the tool needs to perform as advertised. Setting these bounds and expectations is the job of V&V exercises. More precise definitions are given below, but verification can be thought of as the process of determining that a particular numerical algorithm has been implemented as intended (i.e., is bug free), while validation is the process of determining

if the numerical algorithm adequately replicates observations in the physical world. CFD development teams in the industry have always conducted limited V&V to ensure that the algorithm and physical model implementation are correct and functions as intended. As an example, in the 1980s one would implement a shock-capturing scheme and then compute the flow over a simple bi-cone to compare pressure or velocity against experimental data (Bush 1988). Favorable comparisons were considered sufficient evidence of a proper implementation and of the usefulness of the scheme.

Many of these efforts were limited in scope and were point validations against relevant wind tunnel data. Similar to the above V&V process, if there was a reasonable comparison between the CFD prediction and the wind tunnel data, then the code capability was declared validated for the intended application (Mani et al. 1997). In these studies, the wind tunnel data were often considered the truth and the uncertainty in that data was not typically questioned. Today there is much more focus on the uncertainty surrounding the data when judging the agreement between the numerical and experimental sources (uncertainty in both is taken into account). Experimentally, one may consider placing the same model in two different wind tunnels, as was done during the AIAA (American Institute of Aeronautics and Astronautics) Drag Prediction Workshop series, to measure the facility's impact on the data (Levy et al. 2013). Numerically, one may consider the impact of different turbulence models, mesh resolution, numerical algorithm, or even the uncertainty in closure coefficients (Schaefer et al. 2017) within physical models to assess how much the CFD prediction is to be believed. It is also important to distinguish between validation experiments, where additional data are collected for the explicit purpose of completely defining the CFD problem, and tests conducted in support of aircraft design (Oberkampf & Smith 2014). The latter are generally not sufficient for rigorous CFD validation.

**4.1.1. Modern code verification.** Lee et al. (2016) defined verification as “the process of determining that a model implementation accurately represents the developer’s conceptual description of the model and the solution to the model” (p. 3). At Boeing, a rigorous process for verification of the N-S CFD codes began in the last decade. This, combined with complementary validation work, was undertaken to enable use of CFD and wind tunnel data jointly/interchangeably and to establish formal limitations of each code. This verification process is relatively lengthy, tedious, expensive, and generally requires the availability of source code due to its intrusive nature. Aerospace companies also utilize commercially developed/licensed CFD codes that do not come with source code access. This limits the ability of the end user to perform verification exercises and instead necessitates reliance on the vendor to have done an adequate job. The commercial CFD vendors generally consider verification data to be their company’s proprietary information and do not share them with end users. However, the turbulence-modeling resource (TMR) verification site at NASA-LaRC was created by Chris Rumsey to enable nonintrusive verification/benchmarking of various turbulence models (Rumsey 2021). The TMR documents various turbulence models and provides expected solutions of those models to some canonical problems to help verify that the implementation of a particular model is correct in a given code. **Figure 5** shows the expected behavior of the SA (Spalart & Allmaras 1992) and the SA-QCR2000 (SA with quadratic constitutive relation, 2000 version; Spalart 2000) models for flow over a 2D zero-pressure gradient flat plate as a function of grid resolution with a Mach number of 0.2 and a Reynolds number of 5 million. The plot shows that two codes approach the same solution as the mesh error is minimized or eliminated. Implementation of the model in other codes can be verified by comparing to these results. Note that nothing is said here about how well those predictions match reality—that is the job of validation.

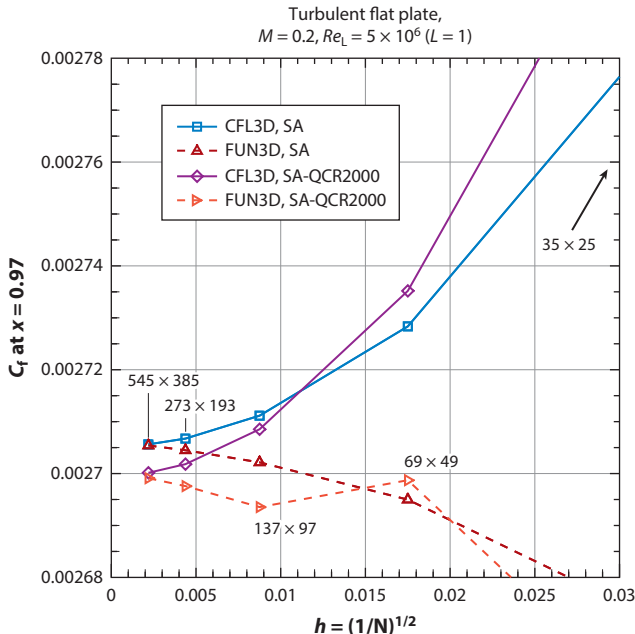


**Figure 5**

Comparison of the SA (Spalart & Allmaras 1992) and the SA-QCR2000 (Spalart 2000) model predictions of the coefficient of friction  $C_f$  at different grid resolutions  $b = (1/N)^{1/2}$ , for Mach number  $M = 0.2$  and Reynolds number per length  $Re_L = 5 \times 10^6$  ( $L = 1$ ). Figure adapted from Rumsey (2021). Abbreviations: CFL3D, Computational Fluids Laboratory 3D; SA, Spalart–Allmaras; SA-QCR2000, SA with quadratic constitutive relation, 2000 version.

**4.1.2. Modern code validation.** Lee et al. (2016) defined validation as “the process of determining the degree to which a model is an accurate representation of the real world from the perspective of the intended uses of the model” (p. 3). Industrial CFD code validation is an ongoing process that is nonintrusive and can be done regardless of source code access. It contains mesh resolution studies and comparisons with wind tunnel and flight test data. The purpose is to understand how well CFD can perform for a range of flight conditions, as well as how well it can predict the effect of geometrical configuration changes throughout the design process.

As a result, and as a consequence of the temporal and financial investment in these exercises, the industry is reluctant to exchange one CFD code for another. Generally, it takes multiple years and multiple engineers to establish validity and the limitations of a code, which can slow the adoption of new tools, even when, for a few cases, the new tool demonstrates superior results. **Figure 6** shows lift coefficient predictions for a high-lift configuration versus angle of attack from multiple RANS codes, along with the same predictions with WMLES (wall-modeled large eddy simulation) codes, Alya, and charLES. While Alya is observed to provide an accurate prediction of pre- and poststall lift for this problem (a fine achievement), the code would need to undergo the laborious effort described above to properly establish the bounds of use over a wide range of flight conditions and geometries. The reluctance of industry to quickly and broadly accept a new CFD code stems from the risk that doing so can introduce into the incredibly expensive design and certification process of a new airplane. This rigorous validation process is a requirement in any effort to obtain industry’s and certifying organizations’ willingness to accept the CFD data in place of other data sources (Walden et al. 2017).

**WMLES:**  
wall-modeled large  
eddy simulation

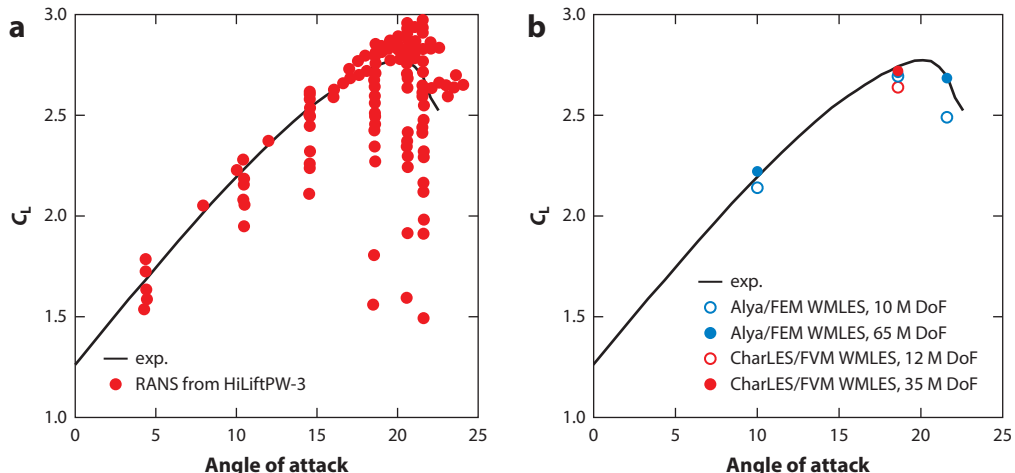


**Figure 6**

Lift coefficient  $C_L$  versus angle of attack from (a) RANS results from HiLiftPW-3 (<https://hiliftpw.larc.nasa.gov/index-workshop3.html>) and (b) two WMLES codes, Alya and CharLES (Lehmkuhl et al. 2019, Goc et al. 2021). Figure adapted from Lehmkuhl et al. (2019). Abbreviations: CFL3D, Computational Fluids Laboratory 3D; exp., experiment; FEM, finite-element method; FVM, finite-volume method; HiLiftPW-3, Third High-Lift Prediction Workshop; M DoF, millions of degrees of freedom; RANS, Reynolds-averaged Navier–Stokes; WMLES, wall-modeled large eddy simulation.

#### 4.2. Geometry Challenges

One of the most fundamental inputs affecting the CFD simulation is the outer moldline (OML) of the aircraft (i.e., the geometry). The OML used for a CFD simulation is generally smooth, defeatured, and watertight. The defeaturing step requires some level of intuition into what features the flow cares about, and it is done to simplify the grid generation process and to accelerate the time required to generate a flow solution. In theory this step can be somewhat enhanced by using grid-generation techniques that effectively shrink-wrap the true geometry, but we have found those to be generally insufficient for design needs in the aerospace industry. Any advancements in this area would provide value to the industry when dealing with detailed geometry with a mature program.

A second challenge comes from the continued development and use of numerical aerodynamic shape-optimization tools. These methods may manipulate the geometry definition directly, but most often they instead manipulate the initial CFD mesh as a surrogate for the true geometry. This latter tactic is often chosen since it is generally more accommodating to impose constraints on the movement of individual vertices than on the analytical curves or surfaces that define the geometry (Taylor & Haines 2018). In this case, the final mesh, which presumably embodies some desirable features, needs to be turned into a form interpretable by the CAD system. While methods have been developed that are sufficient for this purpose, this remains an area for improvement.

Another challenge arises from the increased interest and use of mesh adaptation, and this has heightened awareness of geometric fidelity. In mesh adaptation it is critical to project the adapted grid to the geometry rather than the initial surface mesh to avoid geometric deterioration during mesh refinement. This is a true challenge when dealing with real industrial CAD models, which are only perfect above necessary tolerances. Below these tolerances, there may be gaps or jumps in the surface definition that can inhibit the ability of the adaptation algorithm to complete the intended refinement on the analytical geometry. Robust handling of these situations is a requirement for routine application of useful adaptive mesh technology.

Aside from challenges related directly to the CFD analysis process, tracking and recording the geometry used for a given analysis are essential since computational simulation is playing an increasingly important role at each stage of product life cycle. Variation in geometric fidelity is leveraged to balance simulation accuracy with simulation efficiency and is driven by product maturity and the purpose of the simulation. Geometries of disparate fidelity and content may exist to feed various analyses for different purposes. Tracking and recording the geometry used for a particular analysis, including the intent with which it was conceived, are critical to prevent later misuse of an inappropriate version and to document/quantify the pedigree of a given analysis. As the industry continues to embrace and completely migrate to MBE-based processes, these ideas should be captured and embodied in standard practices. This seems natural given the central role geometry takes in the MBE construct.

### 4.3. Mesh Adaptation

In the mid-1990s CFD utilization was growing rapidly, and some of the meshing challenges had to be addressed. Best practices were created to minimize failures and improve mesh quality, but mesh generation remained a significant burden and was time consuming. Some companies adopted commercial CFD codes that utilized unstructured meshing, while other companies, like Boeing, decided to develop internal unstructured mesh capabilities. Both of these strategies aimed at enabling process automation to reduce the time required to generate a mesh while at the same time opening the door to future efforts that strove to eliminate the dependency of solutions on the mesh creator (namely, mesh adaptation). While similar efforts and strategies were devised for structured grid technology, the adaptation problem for unstructured meshes was seen as more likely to yield the desired end state owing to the arbitrariness of unstructured mesh topology.

Without adaptive meshing technology, CFD simulations of new problems need to resort to mesh refinement studies to establish gridding strategies that yield solutions of sufficient accuracy relative to some stated requirement. An example of this approach, and the solution sensitivity that exists due to mesh resolution in various codes, was shown in the AIAA Drag Prediction Workshops and in the First High-Lift Prediction Workshop (Vassberg et al. 2010, Rumsey et al. 2011). This is a time-consuming step that requires substantial computing power; as a result, it is often skipped in the industry and the analyst's prior experience is relied upon instead. Mesh adaptation technologies intend to eliminate this manual step, automating the mesh placement to yield a prescribed level of solution accuracy.

Boeing made significant investments to develop an anisotropic unstructured mesh adaptation capability called EPIC (Michal & Krakos 2012). Initially, EPIC adaptation was driven by features of the flow (gradients or Hessian matrices of Mach number or pressure). While this does not directly improve the solution accuracy in terms of the quantities of interest (for example, consider supersonic flow over an airfoil in which a feature-based approach would refine the shocks everywhere in the domain, which is unnecessary if the quantity of interest is drag and the shocks are outside of the airfoil's domain of dependence), it provided an input to EPIC that allowed the development of the necessary mesh mechanics and framework. As the capability matured, more error-based metrics were developed to ensure that the adaptation was improving the solution quality. The preferred error metrics are those derived from adjoint solutions of the output of interest (yielding an output-based adaptation). **Figure 7** compares the feature-based and output-based adaptation for drag, where the latter has resolved only features that influence drag on the airfoil (Venditti & Darmofal 2003).

Michal et al. (2021) performed adaptive mesh simulations about a 2D cross section of the NASA High-Lift Common Research Model wing for a range of angles of attack to further understand the behavior of various error estimates. Simulations were computed using a combination of four flow

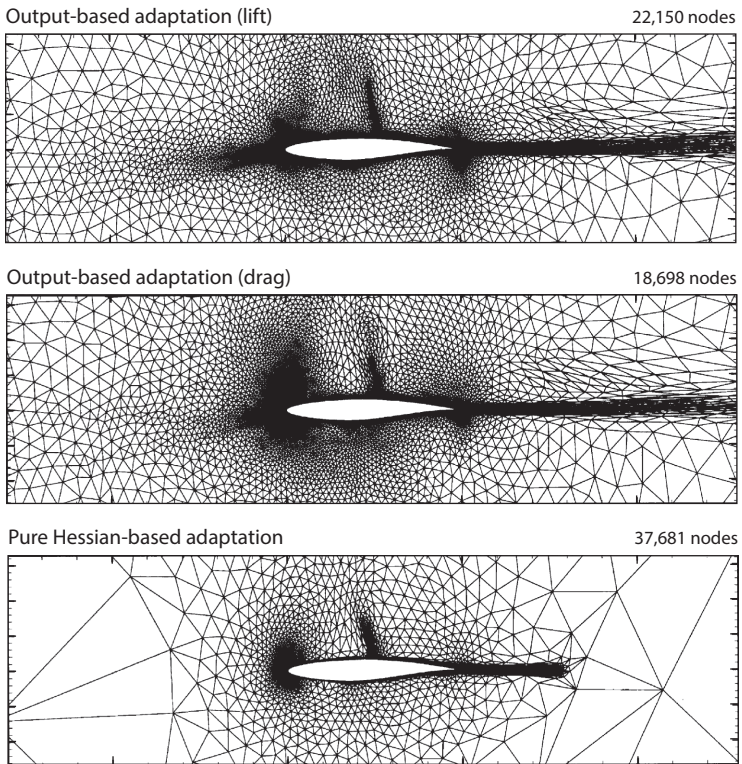


**Figure 7**

Comparison of output-based (*top, middle*) and Hessian (*bottom*) mesh adaptation strategies for an RAE (Royal Aerospace Establishment) airfoil at Mach number  $M = 0.725$  with an angle of attack of  $2.466^\circ$ . Figure adapted from Venditti & Darmofal (2003) with permission; copyright 2003 Elsevier.

solvers, four mesh mechanics methods, and four separate error estimates. The results showed that by continuing the adaptation process to a sufficient level of mesh convergence, nearly identical results could be obtained for any of the adaptive methods regardless of flow solver, mesh mechanics method, or error estimate (see **Figure 8**). However, the results also showed significant differences in the mesh convergence trajectories of the different methods, and these differences can have a significant impact on process efficiency. Output-error-based methods showed a clear advantage in being able to reduce the error to a prescribed level with coarser meshes. More recent Boeing internal studies have also illustrated the advantage of the output-based technique in 3D.

The components of an adaptive CFD process are shown in **Figure 9**. Starting with an initial mesh, a flow solution (and depending on the solver, an adjoint solution) is computed. The information from these flow solutions is used to estimate error and specify a new mesh resolution request via an anisotropic metric field. If the estimated errors are larger than limits specified by the user, the current mesh system is modified to conform to an improved anisotropic metric. Once the adapted mesh is available, the previous flow solution is interpolated to the new mesh to provide an initial condition for the flow solver that approximates the converged solution. The process is repeated until an exit criterion is met (e.g., specified accuracy or allowable run time) (Michal & Krakos 2012). Note that this process essentially places a loop around the Flow Solution step in **Figure 2**, in which the mesh is optimized.

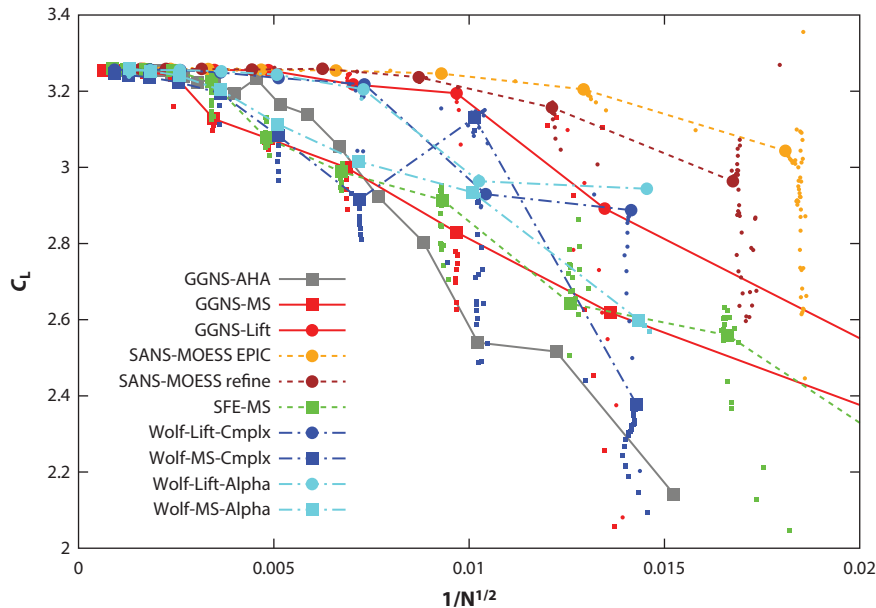


**Figure 8**

Lift coefficient  $C_L$  convergence for an  $\alpha = 8^\circ$  angle of attack for several codes and methods. For full detail and explanation, readers are referred to table 1 of Michal et al. (2021). Figure adapted from Michal et al. (2021) with permission; copyright 2021 American Institute of Aeronautics and Astronautics. Abbreviations: Alpha,  $\alpha$  (angle of attack); AHA, anisotropic heuristic adaptation; EPIC, Edge Primitive Insertion and Collapse; GGNS, general geometry Navier–Stokes; MOESS, Mesh Optimization via Error Sampling and Synthesis; MS, multiscale; SANS, Solution Adaptive Navier–Stokes; SFE, stabilized finite element.

It should be noted that this optimization is conducted for both the surface and volume meshes. Without the surface portion, the usefulness of any such capability would be limited, and we reiterate the essential coupling that is required between the geometry and mesh. These requirements should guide the continued development of geometry and mesh interfaces. Similarly, off-body mesh strategies/requirements further tie the toolsets together. For example, some codes (e.g., those based on finite-element discretizations) may be more tolerant of high anisotropy than others (e.g., those based on finite-volume discretizations). Along similar lines, cell-centered finite-volume discretizations (e.g., as used in BCFD) usually require a mixed-element unstructured grid in which

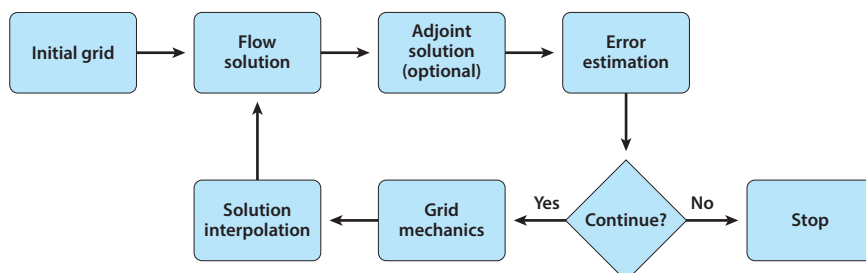


**Figure 9**

Flow chart illustrating the adaptive mesh CFD process. Note the iterative assessment of error and improvement of the mesh until a desired tolerance is reached. Panel adapted from Park et al. (2016).

prismatic or hexahedral elements are stacked in wall-parallel layers to resolve the high shear in the boundary layer. These additional cell types require separate treatment, which is more challenging than mesh adaptation for tetrahedra. Some node-centered finite-volume discretizations use a pure tetrahedral grid (with grid lines orthogonal to the wall), and the same is true of finite-element discretizations. Treating tetrahedra alone generally makes the adaptation problem simpler, and that fact should be a consideration when developing new flow solvers to fit into an adaptive CFD process.

This anisotropic mesh adaptation capability has progressed substantially over the past decade and has begun making impacts within development programs for quality inspections of a limited number of flow conditions within a database. However, routinely applying adaptation for essentially every simulation is still a topic of active research owing to outstanding challenges. There is a great deal of hope for success based on some of the work within the last decade (Park 2008, Michal & Krakos 2012, Alauzet & Loseille 2016), but this area must receive continued investment.

Another area requiring investment, and perhaps a more daunting challenge, is mesh adaptation for unsteady flows. While unsteady flow simulations are routinely conducted within industry today, it is expected that the need for them will increase in the future, especially if certification by analysis (CbA) is to become a reality by 2040 (Slotnick et al. 2014, Mauery et al. 2021). Unsteady flow mesh adaptation will be a critical element in the accurate prediction of the flow field near stall and poststall. However, there are many challenges in making this a reality. For example, simply applying the current techniques used for steady simulations will cause the mesh to lag the flow in time. Therefore, there is a need for space-time adaptation and error estimation. In addition, at each adaptation step, the solution has to be interpolated to the new mesh. This is a significant issue if there are errors in the interpolation process that destroy the time-accuracy of the solution. This process could produce a large cumulative error that overshadows the benefit of the adaptation (Alauzet & Loseille 2016) and grows with integration time.

Having stated all of the above, we recognize that unsteady flow mesh adaptation is an active area of research, and several solutions have been proposed to overcome some of these challenges. Several researchers (Alauzet et al. 2007, Krakos & Darmofal 2010, Fidkowski 2012, Caplan et al. 2019) use temporal windows in which a mesh is used for multiple flow solution time steps before remeshing. This idea minimizes the adaptation time, the cumulative error associated with the solution interpolation, and the memory requirements. Alauzet & Loseille (2016) described a method to extend both feature-based and goal-oriented approaches, developed for RANS, to unsteady anisotropic mesh adaptation.

Unsteady flow output-based mesh adaptation faces an additional challenge: memory (or disk) space. As an example, consider a full aircraft configuration (e.g., **Figure 10**) with 50 million

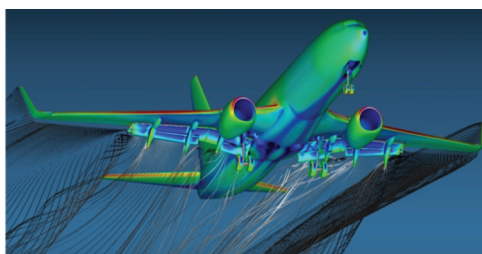


**Figure 10**

CFD simulation of an aircraft in a high-lift configuration. Figure reprinted from Michal et al. (2021) with permission; copyright 2021 American Institute of Aeronautics and Astronautics.

solution points (which is on the low side for industrial applications), with five variables per point. This results in 250 million solution values to be saved (taking up 2 GB, assuming double-precision floating-point representation) per time step to compute the backward sweep through time to determine the adjoint. The memory requirement can be reduced by checkpointing the solutions to disk; however, one must keep in mind the additional time this may add to the overall solution process (Wang et al. 2009). Perhaps a larger concern for output-based unsteady adaptation is that many of the flows that require unsteady analysis are turbulent. In a chaotic process like turbulence, there is incredible sensitivity to the initial conditions of the problem. This is reflected in the adjoint, as the sensitivities blow up as the backward sweep approaches the initial conditions. General techniques for dealing with this fact would be required before this method would be useful for unsteady flow simulations.

#### 4.4. Discretization

The finite-volume method with spatial second-order accuracy and implicit time-stepping is the dominant approach within the aerospace industry, as it has been for years. While some codes claim higher-order spatial accuracy, this usually references the accuracy of the interpolation of data to the boundary of the control volume. While necessary, this is incomplete—the quadrature rule used for integrating the flux through the face must also be improved to realize a formal increase in the order of accuracy. The intent, of course, of developing higher-order algorithms is to reach desired levels of accuracy with smaller meshes. Clearly this would be advantageous to industry if the higher-order algorithm were also sufficiently computationally efficient so as to provide an overall savings in run time and HPC usage. Extending the finite-volume method to third-order accuracy has not shown that benefit for a variety of reasons, both in internal (unpublished) studies in industry and in academic studies (Darmofal & Haimes 2005). However, the compact nature of the finite-element method demonstrates promise.

The results of the First Workshop on Higher-Order Methods was published by Wang et al. (2013) and demonstrated good progress in higher-order finite-element (third-order and higher) methods, illustrating an order-of-magnitude increase (compared to second-order finite-volume methods) in efficiency for the same level of error. However, the workshop also noted that significant challenges remain. One is that in order to realize the benefits of a higher-order flow solution, a higher-order mesh (involving curved edges of the grid cells) is also required. This is necessary because resolving the geometry's curvature with a linear mesh limits the degree to which the mesh can be coarsened, thus hindering the higher-order technique's potential. The workshop also noted challenges with robust solution adaptation, memory usage, and shock capturing. All of these topics are being studied by several researchers and are essential for the ultimate adoption of higher-order methods in industry. For example, there have been notable contributions on shock capturing over the past few years (Sheshadri & Crabil 2015, Couchman et al. 2017, Holst et al. 2019), as well as some recent encouraging work by Ursachi et al. (2020) demonstrating successes with an adaptive CG-VMSD (Continuous Galerkin Variational Multiscale with Discontinuous subscales) method, which shows a computation time that is an order of magnitude less for third- or fourth-order methods' accuracy than for that of industry-standard second-order methods. Just as the industry evolved to adopt second-order finite-volume methods (over earlier first-order discretizations) for its computational efficiency, it is expected that the same will be true of higher-order methods as the challenges noted above continue to be resolved and the methods mature.

Finite-element discretizations have another place in industry, aside from the allure of higher order. The finite-volume codes in use today generally apply a first-order accurate linearization of the residual as part of the implicit time-stepping update algorithm. The lack of a perfect,

consistent linearization of the second-order accurate residual generally prevents complete residual convergence. Since higher-order accuracy in a finite-volume code involves increasing the number of solution points participating in the calculation of a given point's residual (i.e., the stencil), the memory requirement for storing the linearization grows tremendously over first-order memory requirements. However, the compact stencil on which finite-element discretizations are based results in a tolerable increase in memory. The downside (whether finite-volume or finite-element) is that the matrix is harder to solve. Boeing's GGNS code (Kamenetskiy et al. 2014) uses an exact linearization/Jacobian and allows for Newton-like convergence as the solution is approached. This necessitates and is enabled by a strong linear solver built on an ILU (incomplete lower–upper factorization)-preconditioned GMRES (generalized minimal residual method). These methods can provide machine-level convergence of the residual and eliminate errors associated with incomplete convergence.

Unsteady simulations of resolved turbulence are improved by reducing the amount of numerical dissipation introduced in the inviscid flux calculation. Multiple proposals have been made along these lines that alter the flux calculation from its usual form (e.g., Winkler et al. 2012, Nishikawa & Liu 2018). Other approaches define new flux schemes that have different advantageous properties that yield the preservation of kinetic energy or entropy, such as the kinetic energy-preserving scheme (Honein & Moin 2004, Jameson 2008) and the kinetic energy- and entropy-preserving (KEEP) algorithm (Chandrashekhar 2013, Kuya & Kawai 2020). Recently Goc et al. (2021) used charLES with a KEEP scheme and demonstrated accurate prediction of the maximum lift coefficient for the AIAA High-Lift Prediction Workshop configuration.

## 4.5. Turbulence Modeling

In all but the case of direct numerical simulation (DNS), some form of model is required to represent the effect of fluid turbulence on the flow. For large eddy simulation (LES) or detached eddy simulation (DES), a portion of the turbulence is resolved (i.e., captured) both spatially and temporally. In these cases, the turbulence model (or subgrid model) represents the energy contained by structures smaller than some cutoff size. In industry, the most common approaches use the mesh spacing to set the cutoff, and the model is used to provide the effect that turbulent structures smaller than the mesh have on the resolved scales. When the temporal dynamics of the flow is not needed it is more efficient to directly solve for the time-average of the flow via the RANS equations. This is the most common technique applied in industry today, but it puts a great burden on the turbulence model since every effect of the turbulence on the mean flow is the responsibility of the model. The current states of both the steady state and unsteady modeling approaches are discussed below, including their challenges and research needs.

**4.5.1. Steady simulation (Reynolds-averaged Navier–Stokes models).** At Boeing, the workhorse RANS models for design, analysis, and risk mitigation are primarily the SA model (Spalart & Allmaras 1992), its SA-RC (SA with rotation and streamline curvature correction) and SA-QCR variants (Spalart & Shur 1997, Spalart 2000, Mani et al. 2013), and Menter's shear stress transport (SST) model (Menter 1994). Lockheed Martin also has its own proprietary CFD code, Falcon, with the  $k-l$  turbulence model developed by Brian Smith (Smith 1997). While all work well for attached flows, and flows with small amounts of separation, they can be inadequate for other situations dominated by large boundary layer separation, such as those seen at high angles of attack (recall the RANS results shown in **Figure 6**). This is unfortunate given the relative computational efficiency of RANS. In addition to the advancements of the SA model, many other modifications have been studied, but rarely have they provided general improvements. One current and novel idea is the macroscopic forcing method (MFM), which determines the “closure

operators” that govern the mean-field mixing of a given flow field. The MFM model is not based on the Boussinesq (1877) approximation, isotropy, or the separation of scales between turbulence and mean fields. It avoids model-form inaccuracies that plague the primary RANS models in use in the aerospace industry by avoiding tuning constants that limit their application and universality. Additionally, this approach unifies macroscopic modeling between low-Reynolds number laminar flows and high-Reynolds number turbulent flows (Mani & Park 2021). The MFM is still under development and not ready for complex industrial applications; however, it represents a new approach to RANS modeling that has the potential to reinvigorate the hope for accurate RANS simulations in moderately separated flow fields. If realized, it would save a tremendous number of computing hours in industrial applications.

RANS will continue to be a workhorse of aerospace industrial CFD for years to come. Any and all new good ideas are encouraged to be researched and developed. Improving the accuracy or expanding the scope of applicability of our current RANS methods would have a significant impact on the industry.

**4.5.2. Unsteady simulations.** Unsteady flow simulation is also essential for industrial applications, not just for treating regimes where RANS is insufficiently accurate but also for those cases where the time history or dynamics of the flow is of interest or for cases in which there is moving geometry. Within Boeing, this task in years past has fallen to DES (Spalart et al. 1997) where the near-wall flow (i.e., boundary layer) is treated with RANS while the off-body, separated flow is treated with an LES model. Techniques like these are generally called hybrid models, and the use of RANS near the wall avoids the prohibitive cost of resolving the small-scale turbulence within the boundary layer. Aside from the original DES model, which is based on the SA model, others based on SST have been conceived and applied (Bush & Mani 2001; Strelets 2001; Winkler et al. 2011, 2013). While all these methods have been incredibly valuable there are some deficiencies in them as well.

One of the primary deficiencies has come to be called modeled stress depletion (MSD). This is an issue that arises when the transition from RANS to LES happens very near the wall. The grid is not properly refined to resolve the small-scale features present there; hence, the simulation quality is poor and contains too little viscous stress. This generally manifests as grid-induced premature flow separation. The original DES model was particularly sensitive to this phenomenon, making acceptable grid generation challenging (Spalart 2001). This was significantly improved by the delayed DES (DDES) model (Spalart et al. 2006), which added a shielding function devised to detect boundary layer flows and then force the model to remain in RANS mode within them. For this reason, the DDES model is used in almost all circumstances for unsteady flow simulations at Boeing. However, certain grid topologies can still trigger MSD even with the improvements of DDES. These can be particularly challenging for unstructured meshes due to a lack of sufficient control in grid point placement. We also expect it to be an issue as unsteady adaptive mesh techniques mature, unless the mesh adaptation mechanics is somehow aware of the requirements for DDES. Menter (2016) developed a robust shielding function for the two-equation hybrid turbulence models; however, the details of the blending function are proprietary to Ansys. A completely robust shielding function within the public domain would be valuable and mitigate the concerns raised above.

An example of DDES MSD was studied at Boeing on a serpentine inlet geometry (Lakebrink & Mani 2018) with smooth-body separation. The mesh was refined in the region where the boundary layer was expected to separate. Upstream of the separation, the boundary layer was compared to a RANS solution on the same grid, and it was found that the eddy viscosity had substantially decayed within the boundary layer (**Figure 11**). Modification of the  $f_d$  coefficient in the DDES

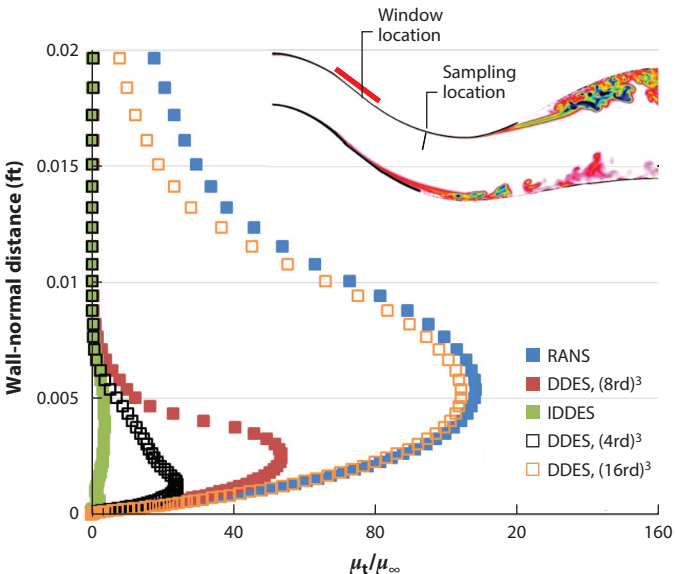


**Figure 11**

Sensitivity of DDES and IDDES models to grid resolution and modeling choices for an attached boundary layer (Lakebrink & Mani 2018), where  $\mu_t/\mu_\infty$  is the ratio of eddy viscosity to the freestream molecular viscosity.  $(8rd)^3$  represents the standard shielding function developed by Spalart, and  $(4rd)^3$  and  $(16rd)^3$  were modifications of the shielding function to investigate its impact. Figure adapted from Lakebrink & Mani (2018) with permission; copyright 2018 The Boeing Company. Abbreviations: DDES, delayed detached eddy simulation; IDDES, improved DDES; RANS, Reynolds-averaged Navier-Stokes.

shielding function from 8 to 16 improved the boundary layer but damped all detached eddies and substantially delayed the separation. This was further investigated by Mani & Winkler (2016) and Ashton (2017), who found that when the surface mesh is nearly isotropic DDES will choose the LES branch in the boundary layer and the solution quality deteriorates. This was also found for the improved DDES model (Shur et al. 2008, Ashton et al. 2016, Lakebrink & Mani 2018).

While hybrid RANS/LES is still a workhorse for most unsteady simulations in industry, it is too expensive to be applied to a large number of flight conditions necessary for building a database, despite efforts to reduce dissipation levels and thus minimize grid requirements (e.g., Winkler et al. 2012). It has also struggled at times to accurately predict the separation/reattachment point in flows with smooth-body separation.

An approach that has shown promise in this regard (and that has been recently developed and tested for industrial application) is WMLES. WMLES is a hybrid approach in its own right (LES is coupled with a wall model, similar to the well-known wall-function treatment used in some RANS codes) and pushes the LES region into the boundary layer. There has been a substantial amount of research on equilibrium and nonequilibrium near-wall modeling for WMLES over the past decade (Cabot & Moin 2000, Balaras & Piomelli 2002, Larsson & Kawai 2010, Larsson & Wang 2014, Park & Moin 2014, Larsson et al. 2016, Schumann et al. 2020) and a relatively recent review given by Bose & Park (2018). Significant progress has been made, and the results are encouraging (Goc et al. 2020, Lozano-Durán et al. 2021), but to make WMLES a routinely used tool for the aerospace industry, we need continued validation on different cases that illustrate mesh-independent predictions of the quantities of interest, studies that define where and when WMLES is the desirable modeling approach, and focus on other related topics. As an example,

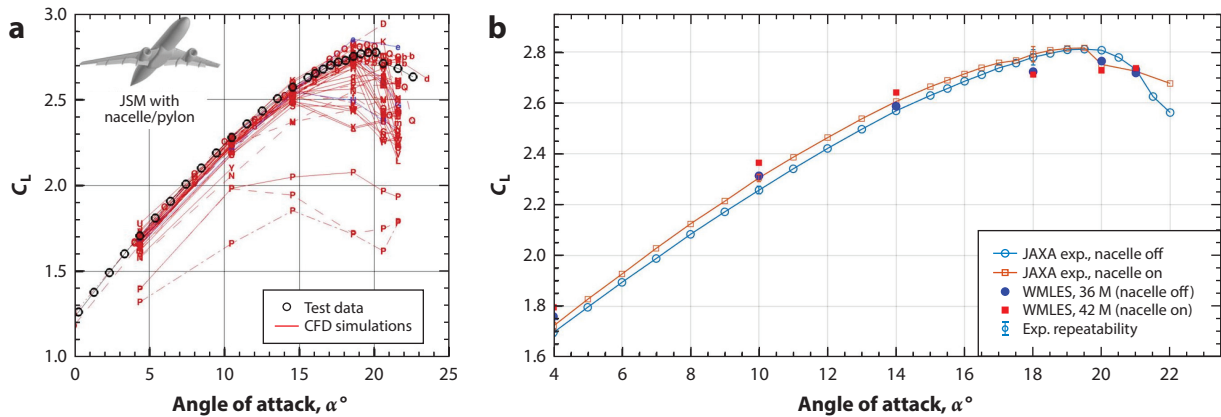


**Figure 12**

(a) Lift coefficient  $C_L$  curve for the JSM configuration comparing experiment (*circles*) and RANS CFD predictions of various codes (*colored points*). Panel adapted from Slotnick et al. (2017). (b) Experimental results compared to WMLES predictions of JSM configuration. Panel adapted from Goc et al. (2020) with permission; copyright 2020 American Institute of Aeronautics and Astronautics. Abbreviations: exp., experiment; JSM, JAXA standard model; M, million; RANS, Reynolds-averaged Navier–Stokes; WMLES, wall-modeled large eddy simulation.

one can look at the results from the Third AIAA High-Lift Prediction Workshop (Rumsey et al. 2019), which utilized a representative wide-body commercial aircraft configured for landing. Results collected from participants in the workshop indicate that, as a whole, RANS may not be adequate in the near-stall/poststall region, with some models and codes dramatically missing the stall behavior (**Figure 12a**). Alternatively, Goc et al. (2020, 2021, 2022) utilized a WMLES technique and predicted the abrupt lift break near the stall (**Figure 12b**). However, the overprediction of lift at lower angles of attack show that further investment and research are needed.

This study, and others like it, indicate that there is a need for additional research/investment in WMLES approaches before they are ready for routine industrial applications. Particular areas of investment for WMLES that we feel would be of great help to industry are the demonstration of mesh independent results for the quantity-of-interest within acceptable tolerance (i.e., wind tunnel uncertainty) and automation of the exchange location identifier between LES and the wall-model-solver (or its elimination). These steps will help identify the long-term role WMLES has within industrial application.

## 5. CHALLENGES AND OUTLOOK

CFD has become a mature technology that industry routinely relies upon as a standard tool. We have witnessed the successful numerical/digital design of aerospace vehicles in recent years, replacing (or at least supplementing) the experimental techniques of the past. Additionally, CFD is sometimes relied upon as the sole source of data for certain aspects of databases in the aerospace industry, including ground effects, throttle-dependent effects, and dynamic derivatives. Airframe loads have been developed using CFD and so have airframe and jet noise estimates. However, none of this is to say that all wind tunnel testing has ever been, will ever be, or should be replaced with computational approaches. Rather, we expect the two to continue to be complementary data sources in the creation of models of a vehicle’s expected flight behavior. This partnership will continue to strengthen, and CFD will be used more routinely and completely to develop and provide the increments to the wind tunnel data needed to correct the results to flight scale, in free air,

and with a powered propulsion system; on many efforts we have already adopted this concept of operations (**Figure 1**). Despite all the reported success stories involving CFD, there have also been plenty of failures and false starts, whether reported or not, as well as remaining challenges that must be addressed in order to continue to evolve CFD technology and further integrate the CFD tools and processes in the digital design framework. Furthermore, the aerospace industry is beginning to consider CbA, for which CFD will be a major source of data in addition to wind tunnel and flight test results. This points to a similar set of challenges that must be overcome in order for CbA to become reality (and all its hopes of providing a new aircraft to the market in a faster, safer, and more cost-effective fashion), some of which are discussed below.

First and foremost, V&V will always be a critical element in the development and deployment of new CFD technologies. However, it is also a critical step toward CbA. Before CFD can provide a significant source of certification data, it is paramount that V&V demonstrations be made on real configurations as opposed to canonical cases. Presently, there are high-quality validation data for canonical cases, but very few high-quality validation-worthy flight test data in the open literature. (The authors acknowledge that collecting these data is not without its own set of challenges.) Many canonical validation tests produce data that are generally for a single discipline. There is a serious shortfall in the high-quality multidisciplinary validation data needed to enable CbA (e.g., coupled fluid–structural unsteadiness in high-lift conditions), and we encourage focus in this area as well. Finally, we find it worthwhile to mention that tests done for the sake of CFD validation are unique—they must collect data, which are otherwise unnecessary, for the sole purpose of allowing the CFD practitioners to completely specify the problem in terms of boundary conditions. Knowing as much as possible about the state of the problem allows for fair judgment of the CFD data.

In V&V exercises (as well as in routine applications and CbA), robust and efficient uncertainty quantification (UQ) techniques are essential to provide a level of confidence, or rightful distrust, of the data. Work on this front has been ongoing for several years, and we encourage continued investments. Developing and advocating for a standard set of accepted practices and UQ descriptors for CFD solutions would be particularly helpful. Additionally, distilling the information and presenting it in ways that can be easily appreciated and interpreted by standard CFD consumers in industry are critical for showing the value of this information and what it brings to the end product.

Part of the uncertainty in CFD solutions comes from the necessity of using a finite grid. The truncation error this introduces corrupts, at some level, the solution of the equations we intend to solve. This uncertainty can be mitigated, controlled, or captured by automated error or output-based grid adaptation. To be regularly applied, however, the adaptation process needs to be efficient and robust. While a great deal of progress has been made toward this state, the aforementioned remaining challenges will require continued focus and investment in the years to come.

Developing algorithms and refactoring codes to take advantage of emerging accelerator-based HPC paradigms (e.g., GPUs) are the current focus of several CFD development teams. These have the demonstrated potential to tremendously reduce the time to solution, even when viewed on an equal-cost basis with today's current hardware options. This potential cannot be ignored, and we suspect that a code's long-term survival will, in no small part, depend on its ability to adapt and take advantage of evolutions in hardware. As these accelerated codes become commonplace, they will revolutionize how CFD can be used in design and certification processes. Steady-state calculations for building aerodynamic databases will be completed in days rather than weeks. Time-accurate simulations of highly separated flows, jet noise, inlet dynamic pressure distortion, etc. will become routine and conducted for many flight conditions, as compared to the relatively sparse treatment that can be afforded today. Utilizing accelerated HPC will also allow high-fidelity CFD to affordably fit into multidisciplinary analysis and optimization processes

that today rely on lower-order models for flow physics. With this jump in computing power, new bottlenecks will be realized in grid generation, postprocessing, and analyzing and archiving data. Advances must also be made in those areas at a commensurate rate in order to capture the full potential of CFD as HPC resources improve. This challenge, along with the others mentioned above, will be overcome through committed collaborations among academia, government labs/research centers, and industry partners.

## DISCLOSURE STATEMENT

The authors are not aware of any biases that might be perceived as affecting the objectivity of this review.

## LITERATURE CITED

- Alauzet F, Frey PJ, George PL, Mohammadi B. 2007. 3D transient fixed point mesh adaptation for time-dependent problems: application to CFD simulations. *J. Comput. Phys.* 222(2):592–623
- Alauzet F, Loseille A. 2016. A decade of progress on anisotropic mesh adaptation for computational fluid dynamics. *Comput.-Aided Des.* 72:13–39
- Ashton N. 2017. *Recalibrating delayed detached-eddy simulation to eliminate modelled-stress depletion*. Paper presented at 23rd AIAA Computational Fluid Dynamics Conference, Denver, CO, AIAA Pap. 2017-4281
- Ashton N, West A, Mendonça F. 2016. Flow dynamics past a 30P30N three-element airfoil using improved delayed detached-eddy simulation. *AIAA J.* 54(11):3657–67
- Balaras UPE, Piomelli U. 2002. Wall-layer models for large-eddy simulations. *Annu. Rev. Fluid Mech.* 34:349–74
- Bose ST, Park GI. 2018. Wall-modeled large-eddy simulation for complex turbulent flows. *Annu. Rev. Fluid Mech.* 50:535–61
- Boussinesq J. 1877. *Essai sur la théorie des eaux courantes*. Paris: Impr. Natl.
- Buning P, Chiu I, Obayashi S, Rizk Y, Steger J. 1988. *Numerical simulation of the integrated space shuttle vehicle in ascent*. Paper presented at 15th Atmospheric Flight Mechanics Conference, Minneapolis, MN, AIAA Pap. 1988-4359
- Bush R. 1988. *A three dimensional zonal Navier-Stokes code for subsonic through hypersonic propulsion flowfields*. Paper presented at 24th Joint Propulsion Conference, Boston, AIAA Pap. 2012-2830
- Bush R, Mani M. 2001. *A two-equation large eddy stress model for high sub-grid shear*. Paper presented at 15th AIAA Computational Fluid Dynamics Conference, Anaheim, CA, AIAA Pap. 2001-2561
- Bush R, Power G, Towne C. 1998. *WIND: the production flow solver of the NPARC Alliance*. Paper presented at 36th AIAA Aerospace Sciences Meeting and Exhibit, Reno, NV, AIAA Pap. 1997-935
- Cabot W, Moin P. 2000. Approximate wall boundary conditions in the large-eddy simulation of high Reynolds number flow. *Flow Turbul. Combust.* 63:269–91
- Caplan P, Haimes R, Darmofal D, Galbraith M. 2019. *Extension of local cavity operators to 3d + t space-time mesh adaptation*. Paper presented at AIAA Scitech 2019 Forum, San Diego, CA, AIAA Pap. 2019-1992
- Cary A, Dorgan A, Mani M. 2009. *Towards accurate flow predictions using unstructured meshes*. Paper presented at 19th AIAA Computational Fluid Dynamics, San Antonio, TX, AIAA Pap. 2009-3650
- Cascade Technol. 2021. *Large-eddy simulation—our secret sauce*. Web Resour., Cascade Technol., Palo Alto, CA.  
<https://www.cascadetechnologies.com/capabilities>
- Cebeci T, Smith A. 1974. *Analysis of Turbulent Boundary Layers*. New York: Academic
- Chakravarthy S, Szema KY, Goldberg U, Gorski J, Osher S. 1985. *Application of a new class of high accuracy TVD schemes to the Navier-Stokes equations*. Paper presented at 23rd Aerospace Sciences Meeting, Reno, NV, AIAA Pap. 2012-165
- Chandrashekar P. 2013. Kinetic energy preserving and entropy stable finite volume schemes for compressible Euler and Navier-Stokes equations. *Commun. Comput. Phys.* 14(5):1252–86
- Cosner R. 1985. *Integrated flowfield analysis methodology for fighter inlets*. Paper presented at Aircraft Design Systems and Operations Meeting, Colorado Springs, CO, AIAA Pap. 1985-3071

- Couchman BL, Darmofal DL, Allmaras S, Galbraith M. 2017. *On the convergence of higher-order finite element methods to weak solutions*. Paper presented at 23rd AIAA Computational Fluid Dynamics Conference, Denver, CO, AIAA Pap. 2017-4274
- Darmofal D, Haimes R. 2005. *Towards the next generation in CFD*. Paper presented at 43rd AIAA Aerospace Sciences Meeting and Exhibit, Reno, NV, AIAA Pap. 2005-87
- Fidkowski K. 2012. *An output-based dynamic order refinement strategy for unsteady aerodynamics*. Paper presented at 50th AIAA Aerospace Sciences Meeting including the New Horizons Forum and Aerospace Exposition, Nashville, TN, AIAA Pap. 2012-77
- Goc KA, Bose S, Moin P. 2020. *Wall-modeled large eddy simulation of an aircraft in landing configuration*. Paper presented at AIAA Aviation 2020 Forum (Online), AIAA Pap. 2020-3002
- Goc KA, Bose ST, Moin P. 2022. *Large eddy simulation of the NASA High-Lift Common Research Model*. Paper presented at AIAA Scitech 2022 Forum, San Diego, CA, AIAA Pap. 2022-1556
- Goc KA, Lehmkuhl O, Park GI, Bose ST, Moin P. 2021. Large eddy simulation of aircraft at affordable cost: a milestone in computational fluid dynamics. *Flow* 1:E14
- Hayes WD. 1947. *Linearized supersonic flow*. Tech. Rep. AL-222, North American Aviation, Los Angeles, CA
- Holst KR, Glasby RS, Erwin JT, Stefanski DL, Coder JG. 2019. *High-order shock capturing techniques using HPCMP CREATE<sup>TM</sup>-AV kestrel*. Paper presented at AIAA Scitech 2019 Forum, San Diego, CA, AIAA Pap. 2019-1345
- Honein AE, Moin P. 2004. Higher entropy conservation and numerical stability of compressible turbulence simulations. *J. Comput. Phys.* 201(2):531–45
- Jameson A. 1987. *Successes and challenges in computational aerodynamics*. Paper presented at 8th Computational Fluid Dynamics Conference, Honolulu, HI, AIAA Pap. 1987-1184
- Jameson A. 2008. Formulation of kinetic energy preserving conservative schemes for gas dynamics and direct numerical simulation of one-dimensional viscous compressible flow in a shock tube using entropy and kinetic energy preserving schemes. *J. Sci. Comput.* 34:188–208
- Jameson A, Caughey D. 1977. *A finite volume method for transonic potential flow calculations*. Paper presented at 3rd Computational Fluid Dynamics Conference, Albuquerque, NM, AIAA Pap. 1977-635
- Jameson A, Schmidt W, Turkel E. 1981. *Numerical solution of the Euler equations by finite volume methods using Runge Kutta time stepping schemes*. Paper presented at 14th Fluid and Plasma Dynamics Conference, Palo Alto, CA, AIAA Pap. 1981-1259
- Johnson FT, Tinoco EN, Yu NJ. 2005. Thirty years of development and application of CFD at Boeing Commercial Airplanes, Seattle. *Comput. Fluids* 34(10):1115–51
- Jones RT. 1946. *Properties of low-aspect-ratio pointed wings at speeds below and above the speed of sound*. Tech. Rep. 835, NACA (Natl. Adv. Comm. Aeronaut.), Washington, DC
- Kamenetskiy DS, Bussoletti JE, Hilmes CL, Venkatakrishnan V, Wigton LB, Johnson FT. 2014. Numerical evidence of multiple solutions for the Reynolds-averaged Navier–Stokes equations. *AIAA J.* 52(8):1686–98
- Krakos JA, Darmofal DL. 2010. Effect of small-scale output unsteadiness on adjoint-based sensitivity. *AIAA J.* 48(11):2611–23
- Kuya Y, Kawai S. 2020. *Stable, non-dissipative and physically-consistent kinetic energy and entropy preserving (KEEP) schemes for compressible flows*. Paper presented at AIAA Scitech 2020 Forum, Orlando, FL, AIAA Pap. 2020-0565
- Lakebrink MT, Mani M. 2018. *Numerical investigation of dynamic distortion and flow control in a serpentine diffuser*. Paper presented at 2018 AIAA Aerospace Sciences Meeting, Kissimmee, FL, AIAA Pap. 2018-1283
- Larsson J, Kawai S. 2010. Wall-modeling in large eddy simulation: length scales, grid resolution and accuracy. In *Annual Research Briefs 2020*, pp. 39–46. Stanford, CA: Cent. Turbul. Res.
- Larsson J, Kawai S, Bodart J, Bermejo-Moreno I. 2016. Large eddy simulation with modeled wall-stress: recent progress and future directions. *Mech. Eng. Rev.* 3(1):15-00418
- Larsson J, Wang Q. 2014. The prospect of using large eddy and detached eddy simulations in engineering design, and the research required to get there. *Philos. Trans. R. Soc. A* 372(2022):20130329
- Lee HB, Ghia U, Bayyuk S, Oberkampf W, Roy CJ, et al. 2016. *Development and use of engineering standards for computational fluid dynamics for complex aerospace systems*. Paper presented at 46th AIAA Fluid Dynamics Conference, Washington, DC, AIAA Pap. 2016-3811

- Lehmkuhl O, Park G, Bose S, Moin P. 2019. Large-eddy simulation of practical aeronautical flows at stall conditions. In *Proceedings of the Summer Program 2018*, pp. 87–96. Stanford, CA: Cent. Turbul. Res.
- Levy D, Laflin K, Vassberg J, Tinoco E, Mani M, et al. 2013. *Summary of data from the Fifth AIAA CFD Drag Prediction Workshop*. Paper presented at 51st AIAA Aerospace Sciences Meeting including the New Horizons Forum and Aerospace Exposition, Grapevine, TX, AIAA Pap. 2013-46
- Lozano-Durán A, Bose ST, Moin P. 2021. Performance of wall-modeled LES for external aerodynamics in the NASA juncture flow. arXiv:2101.00331 [physics.flu-dyn]. <https://doi.org/10.48550/arXiv.2107.01506>
- Mani A, Park D. 2021. Macroscopic forcing method: a tool for turbulence modeling and analysis of closures. *Phys. Rev. Fluids* 6(5):054607
- Mani M, Babcock D, Winkler C, Spalart P. 2013. *Predictions of a supersonic turbulent flow in a square duct*. Paper presented at 51st AIAA Aerospace Sciences Meeting including the New Horizons Forum and Aerospace Exposition, Grapevine, TX, AIAA Pap. 2013-860
- Mani M, Cary A, Ramakrishnan S. 2004. *A structured and hybrid-unstructured grid Euler and Navier-Stokes solver for general geometry*. Paper presented at 42nd AIAA Aerospace Sciences Meeting and Exhibit, Reno, NV, AIAA Pap. 2004-524
- Mani M, Ladd J, Cain A, Bush R. 1997. *An assessment of one-and two-equation turbulence models for internal and external flows*. Paper presented at 28th Fluid Dynamics Conference, Snowmass Village, CO, AIAA Pap. 1997-2010
- Mani M, Winkler C. 2016. *Investigation of shielding parameters in SA/DDES*. Intern. Memo., Boeing, Arlington, VA
- Mauery T, Alonso J, Cary A, Lee V, Malecki R, et al. 2021. *A guide for aircraft certification by analysis*. Contract. Rep. 20210015404, NASA Langley Res. Cent., Hampton, VA
- Mayfield M. 2020. JUST IN: Air Force ‘Digital Century Series’ acquisition concept nearing milestone. *National Defense*, July 14. <https://www.nationaldefensemagazine.org/articles/2020/7/14/air-force-digital-century-series-concept-approaching-new>
- McLean J, Randall J. 1979. *Computer program to calculate three-dimensional boundary layer flows over wings with wall mass transfer*. Contract. Rep. 3123, NASA Langley Res. Cent., Hampton, VA
- Menter FR. 1994. Two-equation eddy-viscosity turbulence models for engineering applications. *AIAA J.* 32(8):1598–605
- Menter FR. 2016. Stress-blended eddy simulation (SBES)—a new paradigm in hybrid RANS-LES modeling. In *Progress in Hybrid RANS-LES Modelling*, ed. Y Hoarau, SH Peng, D Schwamborn, A Revell, pp. 27–37. Cham, Switz.: Springer
- Michal T, Krakos J. 2012. *Anisotropic mesh adaptation through edge primitive operations*. Paper presented at 50th AIAA Aerospace Sciences Meeting including the New Horizons Forum and Aerospace Exposition, Nashville, TN, AIAA Pap. 2012-159
- Michal T, Krakos J, Kamenetskiy D, Galbraith M, Ursachi CI, et al. 2021. Comparing unstructured adaptive mesh solutions for the high lift common research airfoil. *AIAA J.* 59(9):3566–84
- Murman EM, Cole JD. 1971. Calculation of plane steady transonic flows. *AIAA J.* 9(1):114–21
- Nishikawa H, Liu Y. 2018. *Third-order edge-based scheme for unsteady problems*. Paper presented at 2018 Fluid Dynamics Conference, Atlanta, AIAA Pap. 2018-4166
- Oberkampf WL, Smith B. 2014. *Assessment criteria for computational fluid dynamics validation benchmark experiments*. Paper presented at 52nd Aerospace Sciences Meeting, National Harbor, MD, AIAA Pap. 2014-0205
- Park GI, Moin P. 2014. An improved dynamic non-equilibrium wall-model for large eddy simulation. *Phys. Fluids* 26:015108
- Park MA. 2008. *Anisotropic output-based adaptation with tetrahedral cut cells for compressible flows*. PhD Thesis, Mass. Inst. Technol., Cambridge, MA
- Park MA, Loseille A, Krakos J, Michal TR, Alonso JJ. 2016. *Unstructured grid adaptation: status, potential impacts, and recommended investments towards CFD Vision 2030*. Paper presented at 46th AIAA Fluid Dynamics Conference, Washington, DC, AIAA Pap. 2016-3323
- Power G, Cooper G, Sirbaugh J. 1995. *NPARC 2.2 – features and capabilities*. Paper presented at 31st Joint Propulsion Conference and Exhibit, San Diego, CA, AIAA Pap. 1995-2609

- Reyhner T. 1981. Transonic potential flow computation about three-dimensional inlets, ducts, and bodies. *AIAA J.* 19(9):1112–21
- Roe PL. 1981. Approximate Riemann solvers, parameter vectors, and difference schemes. *J. Comput. Phys.* 43(2):357–72
- Rubbert PE. 1994. CFD and the changing world of airplane design. In *ICAS Proceedings 1994*, pp. lvii–lxxxiii. Washington, DC: AIAA
- Rumsey C. 2021. *Turbulence modeling resource*. Web Resour., NASA Langley Res. Cent., Hampton, VA. <https://turbmodels.larc.nasa.gov/>
- Rumsey CL, Slotnick JP, Long M, Stuever R, Wayman T. 2011. Summary of the First AIAA CFD High-Lift Prediction Workshop. *J. Aircr.* 48(6):2068–79
- Rumsey CL, Slotnick JP, Sclafani AJ. 2019. Overview and summary of the Third AIAA High Lift Prediction Workshop. *J. Aircr.* 56(2):621–44
- Schaefer JA, Cary AW, Mani M, Spalart PR. 2017. *Uncertainty quantification and sensitivity analysis of SA turbulence model coefficients in two and three dimensions*. Paper presented at 55th AIAA Aerospace Sciences Meeting, Grapevine, TX, AIAA Pap. 2017-1710
- Schumann JE, Toosi S, Larsson J. 2020. Assessment of grid anisotropy effects on large-eddy-simulation models with different length scales. *AIAA J.* 58(10):4522–33
- Sheshadri A, Crabil JA. 2015. *Mesh deformation and shock capturing techniques for high-order simulation of unsteady compressible flows on dynamic meshes*. Paper presented at 53rd AIAA Aerospace Sciences Meeting, Kissimmee, FL, AIAA Pap. 2015-1741
- Shur ML, Spalart PR, Strelets MK, Travin AK. 2008. A hybrid RANS-LES approach with delayed-DES and wall-modelled LES capabilities. *Int. J. Heat Fluid Flow* 29(6):1638–49
- Slotnick JP, Khodadoust A, Alonso J, Darmofal D, Gropp W, et al. 2014. *CFD Vision 2030 study: a path to revolutionary computational aerosciences*. Contract. Rep. 2014-218178, NASA Langley Res. Cent., Hampton, VA
- Slotnick JP, Wayman T, Simpson D, Fowler S. 2017. *HiLiftPW-3 case 2 results*. Slides presented at 3rd AIAA CFD High Lift Prediction Workshop, Denver, CO, June 3–4
- Smith B. 1997. *A nonequilibrium turbulent viscosity function for the k-l two equation turbulence model*. Paper presented at 28th Fluid Dynamics Conference, Snowmass Village, CO, AIAA Pap. 1997-1959
- Sorenson RL. 1980. *A computer program to generate two-dimensional grids about airfoils and other shapes by the use of Poisson's equation*. Tech. Memo. 81198, NASA Ames Res. Cent., Moffett Field, CA
- Spalart PR. 2000. Strategies for turbulence modelling and simulations. *Int. J. Heat Fluid Flow* 21(3):252–63
- Spalart PR. 2001. *Young-person's guide to detached-eddy simulation grids*. NASA Contract. Rep. 2001-211032, NASA Langley Res. Cent., Hampton, VA
- Spalart PR, Allmaras S. 1992. *A one-equation turbulence model for aerodynamic flows*. Paper presented at 30th Aerospace Sciences Meeting and Exhibit, Reno, NV, AIAA Pap. 1992-439
- Spalart PR, Deck S, Shur ML, Squires KD, Strelets MK, Travin A. 2006. A new version of detached-eddy simulation, resistant to ambiguous grid densities. *Theor. Comput. Fluid Dyn.* 20(3):181–95
- Spalart PR, Jou W-H, Strelets M, Allmaras SR. 1997. Comments on the feasibility of LES for wings, and on hybrid RANS/LES approach. In *Advances in DNS/LES: Proceedings of 1st AFOSR International Conference on DNS/LES*, ed. C Liu, Z Liu, L Sakell, pp. 137–48. Dayton, OH: Greyden
- Spalart PR, Shur M. 1997. On the sensitization of turbulence models to rotation and curvature. *Aerosp. Sci. Technol.* 1(5):297–302
- Stookey D. 2001. *CFD modeling of F/A-18E/F abrupt wing stall—a discussion of lessons learned*. Paper presented at 15th AIAA Computational Fluid Dynamics Conference, Anaheim, CA, AIAA Pap. 2001-2662
- Strelets M. 2001. *Detached eddy simulation of massively separated flows*. Paper presented at 39th Aerospace Sciences Meeting and Exhibit, Reno, NV, 2001-879
- Taylor NJ, Haimes R. 2018. *Geometry modelling: underlying concepts and requirements for computational simulation (invited)*. Paper presented at 2018 Fluid Dynamics Conference, Atlanta, AIAA Pap. 2018-3402
- Thompson JF, Thames FC, Mastin CW. 1974. Automatic numerical generation of body-fitted curvilinear coordinate system for field containing any number of arbitrary two-dimensional bodies. *J. Comput. Phys.* 15(3):299–319

- Tinoco E. 2008. *Validation and minimizing CFD uncertainty for commercial aircraft applications*. Paper presented at 26th AIAA Applied Aerodynamics Conference, Honolulu, HI, AIAA Pap. 2008-6902
- Tramel R, Nichols R. 1997. *A highly efficient numerical method for overset-mesh moving-body problems*. Paper presented at 13th Computational Fluid Dynamics Conference, Snowmass Village, CO, AIAA Pap. 1997-2040
- Ursachi CI, Galbraith M, Allmaras SR, Darmofal D. 2020. *Output-based adaptive RANS solutions using higher-order FEM on a multi-element airfoil*. Paper presented at AIAA Aviation 2020 Forum (Online), AIAA Pap. 2020-3220
- Van Leer B. 1979. Towards the ultimate conservative difference scheme. V. A second-order sequel to Godunov's method. *J. Comput. Phys.* 32(1):101–36
- Vassberg J, Tinoco E, Mani M, Rider B, Zickahr T, et al. 2010. *Summary of the Fourth AIAA CFD Drag Prediction Workshop*. Paper presented at 28th AIAA Applied Aerodynamics Conference, Chicago, AIAA Pap. 2010-4547
- Vatsa VN, Thomas JL, Wedan BW. 1989. Navier-Stokes computations of a prolate spheroid at angle of attack. *J. Aircr.* 26(11):986–93
- Venditti DA, Darmofal DL. 2003. Anisotropic grid adaptation for functional outputs: application to two-dimensional viscous flows. *J. Comput. Phys.* 187(1):22–46
- Verhoff A, O'Neil P. 1981. Extension of FLO codes to transonic flow prediction for fighter configurations. In *Transonic Aerodynamics*, ed. D Nixon, pp. 467–87. Reston, VA: AIAA
- Walden A, Nielsen EJ, Zubair M, Linford JC, Wohlbier JG, et al. 2017. *Unstructured-grid CFD algorithms on many-core architectures*. Poster presented at International Supercomputing Conference for High Performance Computing, Networking, Storage, and Analysis, Denver, CO, Nov. 12–17
- Wang Q, Moin P, Iaccarino G. 2009. Minimal repetition dynamic checkpointing algorithm for unsteady adjoint calculation. *SIAM J. Sci. Comput.* 31:2549–67
- Wang ZJ, Fidkowski K, Abgrall R, Bassi F, Caraeni D, et al. 2013. High-order CFD methods: current status and perspective. *Int. J. Numer. Methods Fluids* 72(8):811–45
- Winkler C, Dorgan A, Mani M. 2011. *Scale adaptive simulations of turbulent flows on unstructured grids*. Paper presented at 20th AIAA Computational Fluid Dynamics Conference, Honolulu, HI, AIAA Pap. 2011-3559
- Winkler C, Dorgan A, Mani M. 2012. *A reduced dissipation approach for unsteady flows on unstructured grids*. Paper presented at 50th AIAA Aerospace Sciences Meeting including the New Horizons Forum and Aerospace Exposition, Nashville, TN, AIAA Pap. 2012-0570
- Winkler CM, Dorgan AJ, Mani M. 2013. *Refinement of a two-equation hybrid RANS/LES model in BCFD*. Paper presented at 21st AIAA Computational Fluid Dynamics Conference, San Diego, CA, AIAA Pap. 2013-3079

## Contents

Flow Computation Pioneer Irmgard Flügge-Lotz (1903–1974) <i>Jonathan B. Freund</i> .....	1
Fluid Mechanics in France in the First Half of the Twentieth Century <i>François Charru</i> .....	11
New Insights into Turbulent Spots <i>Xiaohua Wu</i> .....	45
Self-Propulsion of Chemically Active Droplets <i>Sébastien Michelin</i> .....	77
Submesoscale Dynamics in the Upper Ocean <i>John R. Taylor and Andrew F. Thompson</i> .....	103
Immersed Boundary Methods: Historical Perspective and Future Outlook <i>Roberto Verzicco</i> .....	129
Motion in Stratified Fluids <i>Rishabh V. More and Arezoo M. Ardekani</i> .....	157
The Flow Physics of Face Masks <i>Rajat Mittal, Kenneth Breuer, and Jung Hee Seo</i> .....	193
Advancing Access to Cutting-Edge Tabletop Science <i>Michael F. Schatz, Pietro Cicuta, Vernita D. Gordon, Teuta Pilizota, Bruce Rodenborn, Mark D. Shattuck, and Harry L. Swinney</i> .....	213
Cerebrospinal Fluid Flow <i>Douglas H. Kelley and John H. Thomas</i> .....	237
Fluid Dynamics of Polar Vortices on Earth, Mars, and Titan <i>Darryn W. Waugh</i> .....	265
Dynamics of Three-Dimensional Shock-Wave/Boundary-Layer Interactions <i>Datta V. Gaitonde and Michael C. Adler</i> .....	291

Gas-Liquid Foam Dynamics: From Structural Elements to Continuum Descriptions <i>Peter S. Stewart and Sascha Hilgenfeldt</i> .....	323
Recent Developments in Theories of Inhomogeneous and Anisotropic Turbulence <i>J.B. Marston and S.M. Tobias</i> .....	351
Icebergs Melting <i>Claudia Cenedese and Fiamma Straneo</i> .....	377
The Fluid Mechanics of Deep-Sea Mining <i>Thomas Peacock and Raphael Ouillon</i> .....	403
A Perspective on the State of Aerospace Computational Fluid Dynamics Technology <i>Mori Mani and Andrew J. Dorgan</i> .....	431
Particle Rafts and Armored Droplets <i>Suzie Protière</i> .....	459
Evaporation of Sessile Droplets <i>Stephen K. Wilson and Hannah-May D'Ambrosio</i> .....	481
3D Lagrangian Particle Tracking in Fluid Mechanics <i>Andreas Schröder and Daniel Schanz</i> .....	511
Linear Flow Analysis Inspired by Mathematical Methods from Quantum Mechanics <i>Luca Magri, Peter J. Schmid, and Jonas P. Moeck</i> .....	541
Transition to Turbulence in Pipe Flow <i>Marc Avila, Dwight Barkley, and Björn Hof</i> .....	575
Turbulent Rotating Rayleigh–Bénard Convection <i>Robert E. Ecke and Olga Shishkina</i> .....	603
Nonidealities in Rotating Detonation Engines <i>Venkat Raman, Supraj Prakash, and Mirko Gamba</i> .....	639
Elasto-Inertial Turbulence <i>Yves Dubief, Vincent E. Terrapon, and Björn Hof</i> .....	675
Sharp Interface Methods for Simulation and Analysis of Free Surface Flows with Singularities: Breakup and Coalescence <i>Christopher R. Anthony, Hansol Wee, Vishruth Garg, Sumeet S. Thete, Pritish M. Kamat, Brayden W. Wagoner, Edward D. Wilkes, Patrick K. Notz, Alvin U. Chen, Ronald Suryo, Krishnaraj Sambath, Jayanta C. Panditaratne, Ying-Chih Liao, and Osman A. Basaran</i> .....	707

## **Indexes**

Cumulative Index of Contributing Authors, Volumes 1–55 .....	749
Cumulative Index of Article Titles, Volumes 1–55 .....	760

## **Errata**

An online log of corrections to *Annual Review of Fluid Mechanics* articles may be found at <http://www.annualreviews.org/errata/fluid>